Methane coupling over magnesium oxide: how doping can work

Pierre Schwach, Marc Georg Willinger, Annette Trunschke, and Robert Schlögl*

Functionalization of methane remains a challenging target from academic as well as industrial point of view.[1] New concepts in catalytic activation of C-H bonds are needed[1a] to overcome the current limitations in selectivity, which hamper the broad application of methane coupling in the production of olefins as important platform chemicals from sustainable resources like natural gas or organic waste. Among the various inorganic materials that have been evaluated as heterogeneous catalysts for oxidative coupling of methane (OCM), alkaline earth oxides doped with alkali elements or transition metal ions received particular attention.[2] High reaction temperatures (973-1273 K) are needed. However, the temperature is not required for C-H activation that may aided by coordinatively unsaturated sites already at low temperature,[3] but rather for recovery of an active catalyst surface free of hydroxides and carbonates. Under the harsh reaction conditions, oxide catalysts, like Li-MgO, undergo fast deactivation due to sintering promoted by water as an unavoidable reaction product.[4] Oxygen or magnesium vacancies ($V_O^{··}$, $V_{Mg}^{''}$) are involved in the sintering of MgO by facilitating reconstructions due to enhanced diffusion of lattice ions, which is fast in any case at such high temperatures.[5] On the other hand, vacancies may have an impact on activity and selectivity in catalysis. However, point defects were so far never detected under realistic OCM working condition over MgO.

In a recent study, Freund *et al.* provide evidence that strongly bound O_2^- species as precursor of dissociatively adsorbed O_2 are formed on highly ordered CaO films doped with Mo^{2+}. The results indicate that molecular activation on doped oxides does not require any surface structural defects.[6] Accordingly, it is suggested that activation of methane on smooth surfaces of transition-metal-doped wide-gap oxides may involve such activated oxygen species.

In the present work, we put the concept to test and synthesized powder catalysts, working at T=1023 K. We used doped magnesium oxide as it was frequently investigated in OCM.[7] Pure magnesium oxide deactivates at this temperature quite fast and reaches a stationary state after a few minutes to several hours depending on the applied contact time and the initial nano-structure of the magnesium oxide. In the stationary state, a low, but constant yield of the coupling products ethane and ethene is obtained over smooth, rounded MgO particles.[8]

In this contribution, we introduced Fe in ppm quantity into MgO. The synthesis of Fe-doped polycrystalline magnesium oxide in which the Fe dopant is homogeneously distributed over the entire bulk is, however, quite challenging and requires highly sensitive analytical techniques for verification. The issue is dissolving the dopant in such a way into the bulk of the MgO that no precipitates or segregated nanostructured dopant phases occur during the drastic reaction conditions. Only then the validity of the electronic doping concept put forward by Freund *et al.* can be tested without interference for other catalytic actions of secondary phases.

The presence of Fe atoms on the surface may introduce additional redox chemistry into the activation mechanism of methane, but, even in an ideal solid solution, terminating Fe atoms cannot be avoided. Therefore, the Fe-MgO catalyst was modified by subsequent adsorption of highly dispersed gold on the surface. An Au-MgO catalyst[9] was included in the study for reference.

Table 1. General characteristics of the doped MgO catalysts and normalized formation rates of coupling products ethane and ethene in OCM of methane.

Catalyst	Fe-MgO	Au-Fe-MgO	Au-MgO
ID[a]	14696	14593	14588
c_{Fe}[b] [ppm]	654	402	-
a[c] [Å]	4.214(1)	4.213(1)	4.214(1)
$L_{Vol.}IB$[c] [nm]	46(1)	67(1)	47(1)
A[d] [m²·g⁻¹]	32.0	19.9	25.6
r_{C2+}[e] [µmol·s⁻¹·g⁻¹$_{cat}$]	5.12	13.55	0.68
r_{C2+}[e] [µmol·s⁻¹ m²]	0.16	0.68	0.03
Redox active Fe[f]	6 %	7 %	-

[a] Catalyst ID for clear identification of the batch. [b] Measured by AAS. [c] Determined by XRD. [d] Specific surface area calculated applying the BET equation. [e] Measured after 4 hours time on stream; Reaction conditions: T=1023 K, W/F=0.033 g·s·ml⁻¹, $CH_4/O_2/N_2$=3/1/1. [f] Percentage of Fe that is accessible at the surface as estimated by temperature-programmed reduction (see Tab. S1).

The catalysts were synthesized by hydrothermal treatment of MgO in presence of aqueous solutions of $FeSO_4$, $HAuCl_4$, or a mixture of the two solutions, respectively, in a microwave autoclave at 483 K and 10 bar for 3 hours, followed by annealing in flowing Ar at 1173 K for 3 hours. In order to remove potentially segregated transition metal and metal oxide particles, the obtained solids were subjected to a treatment with aqua regia or nitric acid, respectively, and annealed again in Ar at 1123 K for three hours. X-ray diffraction reveals that the lattice constants of the three doped catalysts do not vary significantly, but the size of the coherently

[*] P. Schwach, Dr. M. Willinger, Dr. A. Trunschke,
Prof. Dr. R. Schlögl
Department of Inorganic Chemistry
Fritz-Haber-Institut der Max-Planck-Gesellschaft
Faradayweg 4-6, D-12489 Berlin (Germany)
E-mail: trunschke@fhi-berlin.mpg.de
Homepage: http://www.fhi-berlin.mpg.de/acnew/welcome.epl

Supporting information for this article is available on the WWW under http://www.angewandte.org or from the author.

scattering domains (reported from full patterns XRD analysis as volume weighted mean column length based on integral breath ($L_{Vol\cdot}IB$)) differs, showing the largest crystalline domains for Au-Fe-MgO, which is also reflected in the lowest specific surface area (Tab. 1). Structural investigation by TEM reveals typical small aggregates consisting of cubic shaped particles that are intergrown and connected mainly along shared faces (Fig. 1). The domain size determined by XRD is similar for Fe-MgO and Au-MgO (Tab. 1) and ranges between 5 and 100 nm according to TEM (Fig. 1). The slightly lower specific surface area of Au-MgO indicates a smoother surface of the gold-covered MgO compared to Fe-MgO.
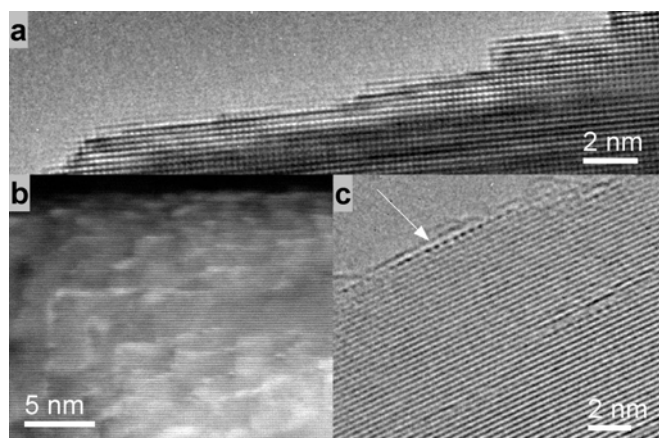

Figure 1. a) HRTEM image showing the stepped surface of Au-Fe-MgO. b) HAADF STEM image with characteristic bright contrast at steps and edges due to decoration with heavy atoms. c) Columns of heavy atoms can also be seen in thin regions in HRTEM.

The UV-vis spectra of Fe-MgO and Au-Fe-MgO are dominated by an intense absorption in the range of ligand to metal charge transfer (LMCT) bands (Fig. S1). The absorption maximum near 288 nm (34723 cm^{-1}) is attributed to isolated Fe^{3+} ions in octahedral coordination, *i.e.*, on Mg^{2+} lattice positions.[10] EPR spectroscopy confirms the occurrence of Fe^{3+} in cubic symmetry sites in MgO (Fig. S2). Contributions of oligomeric species and iron oxide nano-particles to the UV-vis spectra cannot be excluded due to the complex fine structure and the extended tail of the bands towards decreasing energy. However, no aggregates of iron have been detected by TEM, indicating high Fe dispersion. Since the Fe concentration is low, the weak absorption due to d-d transitions in the range between 330 nm (30000 cm^{-1}) and 1000 nm (10000 cm^{-1}) gives featureless, very weak and broad bands that do not allow an unambiguous interpretation with respect to the coordination environment of Fe^{3+} (d^5) ions, and potentially appearing Fe^{2+} (d^6) ions. The spectra of the gold-containing catalysts exhibit the characteristic surface Plasmon mode around 520 nm (19230 cm^{-1}) that is ascribed to gold nano-particles.[11] The broad appearance of the band suggests that Au occurs in different particle sizes ranging from atomic dimensions to Au particles with a diameter of about 10 nm.[12] Indeed, very rare and scarcely distributed isotropic gold nanoparticles can be found on the surface of the MgO particles by TEM.

Temperature-programmed reduction (TPR) – oxidation (TPO) cycles have been performed to analyze the redox properties of the Fe-containing MgO catalysts (Figs. S3-S4). In the first run, the catalysts were heated in inert gas and evolution of hydrogen was observed in a temperature range between 573 and 673 K and under

isothermal conditions at 1073 K indicating the formation of point defects in the bulk of Fe-MgO and Au-Fe-MgO during the thermal pretreatment.[13] The hydrogen-consumption profile of the first TPR run differs from the second and third run that have been performed in each case after intermediate temperature-programmed oxidation. In contrast, the second and third TPR profiles are identical revealing high reversibility, stability and absence of segregation processes after initial stabilization during the first cycle. This applies to Fe-MgO (Fig. S3) as well as to Au-Fe-MgO (Fig. S4) indicating that the catalysts are well comparable, in particular, because the bulk oxide properties, which have been sensed by redox probing, are quite similar in agreement with the XRD results. The first TPR run reveals a dopant-induced difference between the two catalysts. In addition to the two high-temperature peaks around 810-840 K and 1050-1060 K, Fe-MgO exhibits an additional hydrogen consumption peak at low temperature (513 K) arising from easily reducible Fe species. The peak does not appear again in following cycles indicating the dissolution of the species into the bulk where it is protected from re-oxidation. The amount of consumed hydrogen proves that only a minor fraction of the low-level iron doping is susceptible to reduction on the surface (Tab. 1 and Tab. S1) indicating the homogeneous distribution of the dopant within the bulk of magnesium oxide. The fraction of reducible iron is initially higher in Fe-MgO compared to Au-Fe-MgO, indicating that surface iron species are shielded by topping gold species.
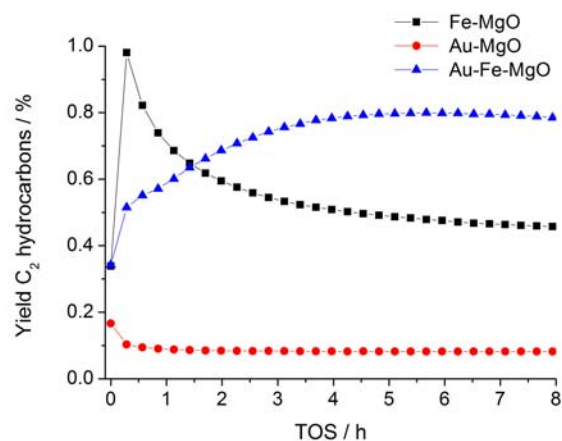

Figure 2. Yield of ethane and ethene in the oxidative coupling of methane as a function of time on stream (TOS) at T=1023 K; W/F= 0.0167 $g\cdot s\cdot ml^{-1}$; $CH_4/O_2/N_2$=3/1/1.

The low yield of coupling products in OCM as presented in Fig. 2 was deliberately measured at short contact times to prevent full oxygen conversion and thus to allow a meaningful kinetic comparison. Gold seems to block the active sites on the surface of MgO since Au-MgO shows only negligible activity. This is ascribed to the propensity of gold to adsorb at step edges of the MgO and thus covering the active sites related to edges.[14] Fe-MgO is more active (Figs. S5-6) and selective (Fig. S7) resulting in higher yield. The start-up behaviour of Fe-MgO is attributed to the presence of surface redox-active iron species in accordance with the observations made by TPR. Further increase in methane conversion and selectivity is achieved by co-doping with Fe and Au. Such a synergistic effect of the two transition metal additives becomes even more obvious by comparing the rate of C_2 formation normalized to the specific surface area of the catalyst (Tab. 1). After a formation

period with increasing activity, Au-Fe-MgO shows stable activity at the time scale of the present experiment. This behaviour is surprising and novel for alkaline earth metal oxide-based catalysts.

An explanation may be provided by electron microscopy. HAADF STEM, which is sensitive to variations in atomic weight, allows locating the heavier dopant atoms in the MgO matrix. As can be seen in Fig. 1, corners and edges are characterized by brighter contrast, indicating the presence of either Au or Fe. This is confirmed by HRTEM images recorded from thin regions of MgO crystals, where rows of strongly scattering atoms are detected at surface steps even after catalytic testing (Fig. 1c and Fig. S8). These atoms will suppress the action of steps as active sites and thus poison the Au-MgO catalyst that does not have sites caused by electronic doping. In addition, investigation of the bulk structure by HAADF STEM and TEM reveals the presence of local strain, causing particular contrast variations such as indicated in Fig. 3a and b, respectively. Analysis of the lattice fringes[15] shows doping induced strain and lattice rotation, as visualized in Fig. 3c and d, respectively. Due to the low concentration, EDX elemental analysis is not sensitive enough to clarify weather the defects are caused by gold or iron incorporation into the MgO lattice.
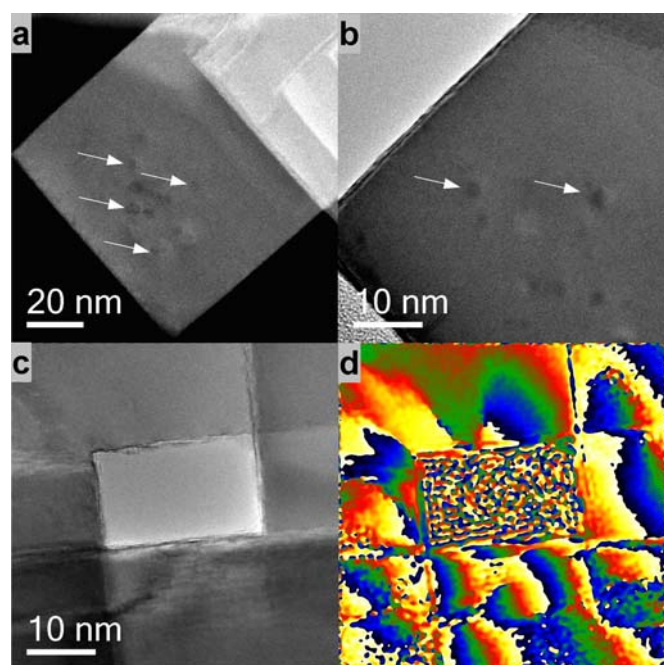

Figure 3. a) HAADF STEM and b) TEM image with localized contrast variations due to defects caused by bulk doping as indicated by arrows. c) HRTEM image of doped MgO particles for which the lattice rotation due to strain is shown in d).

The sintering behaviour of Au-Fe-Mg O is similar compared to un-doped MgO. Initially, the surface of the cube-shaped particles exposed stepped and atomically flat planes (Fig. 1). Steps are usually in the range of half (one atom) and single unit cell height (Fig. 1a). During catalytic reaction, the abundance of such small steps decreases forming larger steps. Despite these sintering phenomena, the catalytic activity of the Au-Fe-MgO catalyst shows appreciable stability. This is a clear indication that the lasting activity is not due to the conversion of methane at steps but rather at sites located at terraces. Doping has changed the nature of the active sites as indicated clearly by the temporal evolution of the catalytic activity shown in Figures 2 and S5-7. The inverse trend for the co-doped system as compared to the other systems points to the

formation of active sites for oxygen activation in Au-Fe-MgO during time on stream whereas the other systems deactivate through the loss of monatomic step sites following surface transformation caused by the reaction products water and CO_2. The stable minimal activity of the Au-MgO system marks the intrinsic activity of active sites in the present MgO that are not associated with step edges. Compared to this activity (see Table 1) the electronic doping by Fe increases the rate of C_2 formation by over an order of magnitude.

For the classical Au-MgO system it was found that small doping levels produce metallic and some chemically active gold species decorating steps and thus reducing the activity of parent MgO exactly as found in the present study.[9] Only at much higher doping levels catalytic effects were described and associated with Au particles and defect formation in MgO. In the present study two types of gold were evidenced based on the catalytic results: In single doped Au-MgO only the step-decorating poisoning effect was found. Through the presence of sub-surface iron species in the co-doped system the edge decorating effect was massively overruled by a beneficial effect of creating structurally stable novel active sites at terraces of the MgO without introducing vacancies that may destabilize the system at longer time on stream. This second gold species apparently arises from a significant gold-support interaction achieved by the strain in the MgO due to iron doping. The possible effects of isotropic unstrained gold particles are negligible in the present study due to their very low abundance as a consequence of the synthesis strategy. Electronic doping of MgO terraces is also achieved through iron dissolution only, but with significant lower effectiveness. It is tempting to conclude that the co-doping creates highly active sites for oxygen activation into a peroxy-species[16] whereas iron doping ends up with sites creating oxo species being less active in creating methyl radicals for OCM.

The purpose of the present work was to elucidate much along the demand of Hutchings[17] how electronic promoters may change the reaction pathway of the OCM reaction. Stimulated through the clear-cut model observation of Freund *et al.* we synthesized a polycrystalline form of model compound exhibiting the same sub-surface doping as evidently achieved in the model system of Freund. By carefully avoiding the formation of nanoparticles of the transition metal oxide we observed the predicted doping effect without interference form deep oxidation of the methane molecule.

It was not our intention to explore the potential of this electronic effect with respect to selectivity and yield. We rather wanted to demonstrate by a catalytic experiment that as from chemical physics predicted an electronic doping effect exists for alkali earth oxides affecting oxygen activation. Its amplification by gold being activated through a specific interaction with MgO at iron-modified sites is an additional benefit. As the doping procedure is reproducible and the levels of doping species are low it is conceivable that the concept of homogeneous electronic doping of alkali earth oxides may find application for stabilization of realistic systems.

Experimental Section

Detailed information on catalyst synthesis, characterization, and catalytic tests is provided in the Supporting Information.

[1] a)H. Schwarz, *Angewandte Chemie International Edition* **2011**, *50*, 10096; b)C. Hammond, S. Conrad, I. Hermans, *ChemSusChem* **2012**, *5*, 1668.

[2]   U. Zavyalova, M. Holena, R. Schlögl, M. Baerns, ChemCatChem **2011**, 3, 1935.

[3]   T. Ito, T. Watanabe, T. Tashiro, K. Toi, *Journal of the Chemical Society-Faraday Transactions I* **1989**, *85*, 2381.

[4]   a)U. Zavyalova, M. Geske, R. Horn, G. Weinberg, W. Frandsen, M. Schuster, R. Schlögl, *ChemCatChem* **2011**, *3*, 949-959; b)U. Zavyalova, G. Weinberg, W. Frandsen, F. Girgsdies, T. Risse, K. P. Dinse, R. Schloegl, R. Horn, *ChemCatChem* **2011**, *3*, 1779-1788.

[5]   D. Beruto, A. W. Searcy, R. Botter, M. Giordani, *The Journal of Physical Chemistry* **1993**, *97*, 9201-9205.

[6]   Y. Cui, N. Nilius, X. Shao, M. Baldofski, J. Sauer, H.-J. Freund, Angewandte Chemie **2013**, submitted.

[7]   J. H. Lunsford, *Angewandte Chemie International Edition in English* **1995**, *34*, 970-980.

[8]   J. S. J. Hargreaves, G. J. Hutchings, R. W. Joyner, C. J. Kiely, *Journal of Catalysis* **1992**, *135*, 576-595.

[9]   K. Blick, T. D. Mitrelias, J. S. J. Hargreaves, G. J. Hutchings, R. W. Joyner, C. J. Kiely, F. E. Wagner, *Catalysis Letters* **1998**, *50*, 211-218.

[10]   G. Lehmann, *Z. Phys. Chem. Neue Folge* **1970**, *72*, 279-297.

[11]   C. F. Bohren, D. R. Huffman, Absorption and Scattering of Light by Small Particles, John Wiley and Sons, New York, **1983**.

[12]   K. C. Grabar, R. G. Freeman, M. B. Hommer, M. J. Natan, *Analytical Chemistry* **1995**, *67*, 735-743.

[13]   B. V. King, F. Freund, *Physical Review B* **1984**, *29*, 5814-5824.

[14]   J. S. J. Hargreaves, G. J. Hutchings, R. W. Joyner, C. J. Kiely, *Catalysis Today* **1992**, *13*, 401-407.

[15]   M. J. Hytch, E. Snoeck, R. Kilaas, *Ultramicroscopy* **1998**, *74*, 131.

[16]   P. Landon, P. J. Collier, A. J. Papworth, C. J. Kiely, G. J. Hutchings, *Chemical Communications* **2002**, *0*, 2058.

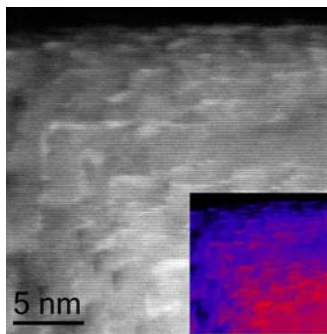[17]   G. J. Hutchings, *Catalysis Letters* **2001**, *75*, 1.

Entry for the Table of Contents

Layout 1:

C-H activation

Pierre Schwach, Marc Willinger, Annette Trunschke*, and Robert Schlögl

Methane coupling over doped magnesium oxide: how doping can work

Oxidative coupling of methane over magnesium oxide is affected by electronic doping creating highly active sites by co-modification of MgO with iron and gold in ppm quantity.

Methane coupling over magnesium oxide: how doping can work

Pierre Schwach, Marc Willinger, Annette Trunschke*, Robert Schlögl

1. Experimental Details

1.1. Catalyst synthesis

Fe-MgO: Two Teflon autoclaves with a volume of 100 mL were filled each with 3 g MgO (Alfa Aesar 99.998 m.b. (ID#14564, batch number 24686) suspended in 69.5 mL distilled water. Subsequently, 0.537 mL of a 0.05 M $FeSO_4$ (Sigma) solution was added. The suspension was heated to 483 K for 3 hours in a microwave oven (Speedwave MWS-3+, Berghof Products + Instruments GmbH) at a pressure of 10 bar. The resulting material was isolated by filtration, washed with distilled water, and dried at 393 K in air for 12 h. For thermal treatment, the dried product was placed into a quartz crucible, which was located inside a quartz tube, and annealed in flowing Ar (150 mL/min) at 1173 K (heating rate 10 K/min) for 3 hours using a tube furnace (Carbolite). To remove segregated iron oxide particles, the resulting solid was washed in a mixture of 5 mL 0.1 M HNO_3 and 25 mL H_2O by stirring at 293 K for 1 hour. The washed and dried product was annealed again in flowing Ar (150 mL/min) at 1123 K (heating rate 5 K/min) for 3 hours.

Au-MgO: Two Teflon autoclaves with a volume of 100 mL were filled each with 3 g MgO (Alfa Aesar 99.998 m.b. (ID#14564, batch number 24686) suspended in 69.5 mL distilled water. Subsequently, 0.51 mL of a 0.015 M $HAuCL_4 \cdot xH_2O$ (Sigma) solution was added. The suspension was heated to 483 K for 3 hours in a microwave oven (Speedwave MWS-3+, Berghof Products + Instruments GmbH) at a pressure of 10 bar. The resulting material was isolated by filtration, washed with distilled water, and dried at 393 K in air for 12 h. For thermal treatment, the dried product was placed into a quartz crucible, which was located inside a quartz tube, and annealed in flowing Ar (150 mL/min) at 1173 K (heating rate 10 K/min) for 3 hours using a tube furnace (Carbolite). To remove segregated Au particles, the resulting solid was washed in a mixture of 5 mL 0.1 M *aqua regia* and 25 mL H_2O by stirring at 293 K for 1 hour. The washed and dried product was annealed again in flowing Ar (150 mL/min) at 1123 K (heating rate 5 K/min) for 3 hours. The resulting catalyst was stored under argon and freshly pre-treated before analysis or catalysis.

Au-Fe-MgO: Two Teflon autoclaves with a volume of 100 mL were filled each with 3 g MgO (Alfa Aesar 99.998 m.b. (ID#14564, batch number 24686) suspended in 69 mL distilled water. Subsequently, 0.508 mL of a 0.015 M $HAuCL_4 \cdot xH_2O$ (Sigma) solution, and 0.538 mL of 0.05 M $FeSO_4$ (Sigma) solution were added. The suspension was heated to 483 K for 3 hours in a microwave oven (Speedwave MWS-3+, Berghof Products + Instruments GmbH) at a pressure of 10 bar. The resulting material was isolated by filtration, washed with distilled water, and dried at 393 K in air for 12 h. For thermal treatment, the dried product was placed into a quartz crucible, which was located inside a quartz tube, and annealed in flowing Ar (150 mL/min) at 1173 K (heating rate 10 K/min) for 3 hours using a tube furnace (Carbolite). To remove segregated iron oxide and Au particles, the resulting solid was washed in a mixture of 10 mL 0.1 M *aqua regia* and 20 mL H_2O by stirring at 293 K for 1 hour. The washed and dried product was annealed again in flowing Ar (150 mL/min) at 1123 K (heating rate 5 K/min) for 3 hours. The resulting catalyst was stored under argon and freshly pre-treated before analysis or catalysis.

The resulting catalysts were stored under argon and freshly pre-treated before analysis or catalysis.

1.2. X-ray diffraction

XRD was measured on a STOE STADI-P transmission diffractometer with a focusing primary Ge(111) monochromator and a linear PSD applying Cu $K_{\alpha 1}$ radiation (λ=1.5406 Å).

The XRD data were analyzed by full pattern fitting using the TOPAS software (version 3, copyright 1999, 200 Bruker AXS).

1.3. Nitrogen adsorption

The surface area determination was carried out in a volumetric N_2 physisorption set-up (Autosorb-6-B, Quantachrome) at the temperature of liquid nitrogen. The sample was degassed in dynamic vacuum at a temperature of 473 K for 2 h prior to adsorption. The relative N_2 pressure was varied (p/p_0=0.05–0.3), and 11 data points were measured. The linear range of the adsorption isotherm was considered to calculate the specific surface area according to the BET method.

1.4. Atomic Absorption Spectroscopy (AAS)

The iron content was determined by Atomic Absorption Spectroscopy (AAS). Experiments were performed on a Perkin Elmer AAS 4100 spectrometer using a N_2O-acetylene flame and a wavelength of 271.9 nm. 250 mg of the catalyst were dissolved in

25 mL HNO_3 (65 % p.a.) and backfilled to 250 mL with distilled H_2O. Zero, 50 and 100 μg iron were added to 25 mL of this solution, respectively, and backfilled to 50 mL with a solution of 5% HNO_3 in water.

1.5. Diffuse reflectance spectroscopy (DRS)

The *in situ* UV-VIS experiments were performed in the range between 200 and 800 nm using a Perkin Elmer Lambda 650 spectrometer equipped with a diffuse reflectance accessory (Praying Mantis, Harrick) complete with an environmental chamber attachment (Harrick HVC-VUV-4) using Spectralon® as white standard. The catalysts were pretreated *in situ* at 923 K for 30 min in flowing Ar (20 mL/min), and measured in the same argon flow at room temperature.

1.6. Electron Paramagnetic Resonance (EPR)

EPR spectra were recorded at liquid nitrogen temperature on a Bruker ESR 300 E spectrometer equipped with a microwave bridge Bruker ER 042 MRH E. A Bruker ER 4116 DM resonator operating in the TE 102 mode (resonance frequency ≈ 9.5 GHz) was used. The spectra were recorded with a modulation frequency of 100 kHz and a microwave power of 2 mW. The frequency and g values were calibrated using the signal of Mn^{2+} ions ($g = 2.0007$, $A = -244$ MHz, $a = 55$ MHz)[S1a] present as impurity in MgO (3 ppm as determined by ICP-OES analysis) A small signal assigned to Cr^{3+} can also be observed with a g tensor of 1.98 (0.2 ppm as determined by ICP-OES analysis). [S1b] The samples were placed in a quartz cell equipped with Teflon Duran® valves and connected to a vacuum system that allows the dosing of gases. Before the EPR measurements, the MgO samples were activated at 1073 K under dynamic vacuum ($10^{-6} – 10^{-7}$ mbar) for 3 hours.

[S1] a) W. Low, *Physical Review* **1957**, *105*, 793-800; b) S. Eidels-Dubovich, V. Beltran-Lopez, *J. Magnet. Res.* **1987**, *74*, 94-104.

1.7. Temperature-Programmed-Reduction-Oxidation (TPR-O) experiments

Temperature-programmed oxidation and reduction experiments were performed in a fixed-bed quartz reactor placed inside a tube furnace (Carbolite). The position of the catalyst inside the reactor was fixed applying a frit. The temperature was measured in the catalyst bed using a thermocouple (K-type). The feed was composed of 0.5 % O_2 or H_2, respectively, in He and Ar, respectively. A flow rate of 90 mL·min^{-1} was applied. A mass of 600 mg of the catalyst with a 200 – 300 μm sieved fraction was used and diluted with 3 g SiC in order to improve the thermal conductivity in the catalyst bed. The measurements were performed applying a heating rate of 10 K·min^{-1}. Hydrogen concentration in the gas phase was analyzed using a TCD detector (Rosemount Analytical) after the off-gas passed a molecular sieve trap to remove water. Before measurements, the catalysts were pretreated in 90 mL·min^{-1} Ar at 1073 K with a heating rate of 10 K·min^{-1} for 1 h to remove adsorbed water molecules and other adsorbates.

1.8. Catalytic measurements

The catalytic measurements were carried out in a laboratory quartz U-tube fixed bed reactor (4 mm inner diameter, 6 mm outer diameter, 26 cm length) applying reaction conditions as indicated in the main text. Gas analysis was performed by online gas chromatography (GC 6890A, Agilent). Nitrogen was used as internal standard to account for volume effects due to the high temperature.

1.9. Electron microscopy

Electron microscopy was carried out using a Cs-corrected FEI Titan 80-300 instrument operating at 300 kV in bright field high-resolution transmission electron microscopy (HRTEM) and high angle annular dark field scanning transmission electron microscopy (HAADF STEM) mode, respectively.
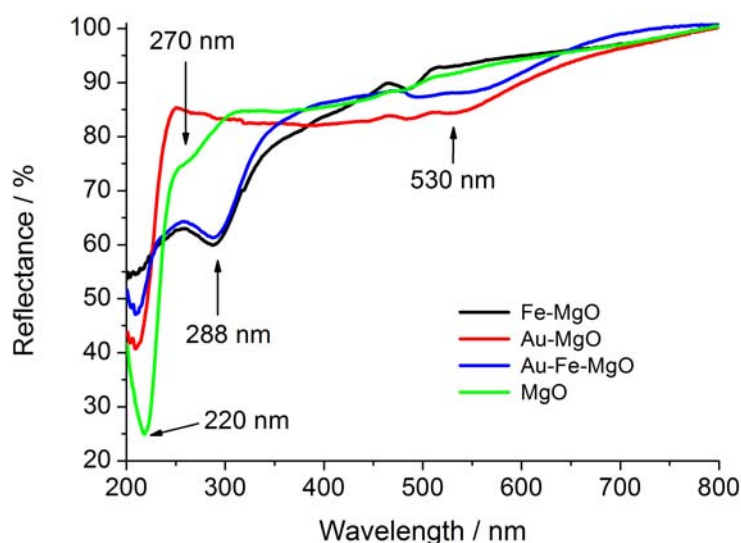
2. Diffuse reflectance spectroscopy

Fig. S1. UV-vis spectra of the doped catalysts measured in Ar at 293 K after pretreatment in Ar at 923 K.
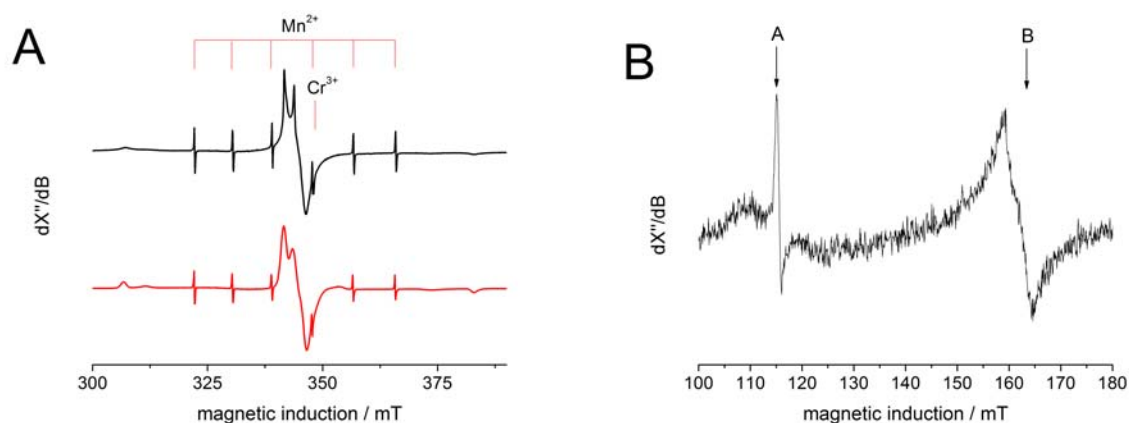
3. EPR spectroscopy

Fig. S2. EPR spectrum of Au-Fe-MgO after pretreatment at 1073 K under high vacuum, measured at 77 K, A) Experimental (black line) and simulated[S2] spectrum (red line). B) Experimental spectra of Fe^{3+} at lower magnetic field. Both spectra are measured at a frequency of 9.63637 GHz.

The experimental signal (Fig. S2 A, black line) at g=2.0037 is attributed to Fe^{3+} ions present in a cubic symmetry field,[S3] which is also well reflected by the simulation of the spectrum (g=2.0037, a=640 MHz, lwpp=1 mT, and D=-100 MHz) using the Easyspin package in MATLAB.[S2] The species A and B at low fields (Fig. S2 B) are assigned to Fe^{3+} ions in a coordination geometry of lower symmetry. These signals are usually assigned to Fe^{3+} in orthorhombic or tetragonal symmetry sites in MgO.[S4] No sign of point defect can be found in the Au-Fe-MgO sample by EPR. [S5]

[S2]   S. Stoll, A. Schweiger, *Journal of Magnetic Resonance* **2006**, *178*, 42-55.

[S3]   aV. Beltrán-López, J. Castro-Tello, *Journal of Magnetic Resonance (1969)* **1980**, *39*, 437-460; bJ. H. Lunsford, *The Journal of Chemical Physics* **1965**, *42*, 2617-2618.

[S4]   J. T. Castner, G. S. Newell, W. C. Holton, C. P. Slichter, *The Journal of Chemical Physics* **1960**, *32*, 668-673.

[S5]   a) R. S. d. Biasi, *Journal of Physics C: Solid State Physics* **1981**, *14*, 4885; b) R. S. De Biasi, A. Caldas, *J. Phys. C: Solid State Phys.* **1977**, *10*, 107-111.

4. Temperature-programmed- reduction-oxidation (TPR-TPO)

Table S1: Hydrogen consumption in TPR (H_2 evolution during activation (negative values)).

	Hydrogen consumption (evolution) /μmol(H_2)/(s·g$_{cat}$)	Fraction of total Fe /%
Au-Fe-MgO	Fe content*: 7.20 μmol/g	
Activation	- 0.25	-
TPR1	0.13	1.8
TPR2	0.48	6.7
TPR3	0.48	6.7
Fe-MgO	Fe content*: 11.71 μmol/g	
Activation	- 0.56	-
TPR1	0.81	6.9
TPR2	0.75	6.4
TPR3	0.74	6.3

* Analyzed by AAS.
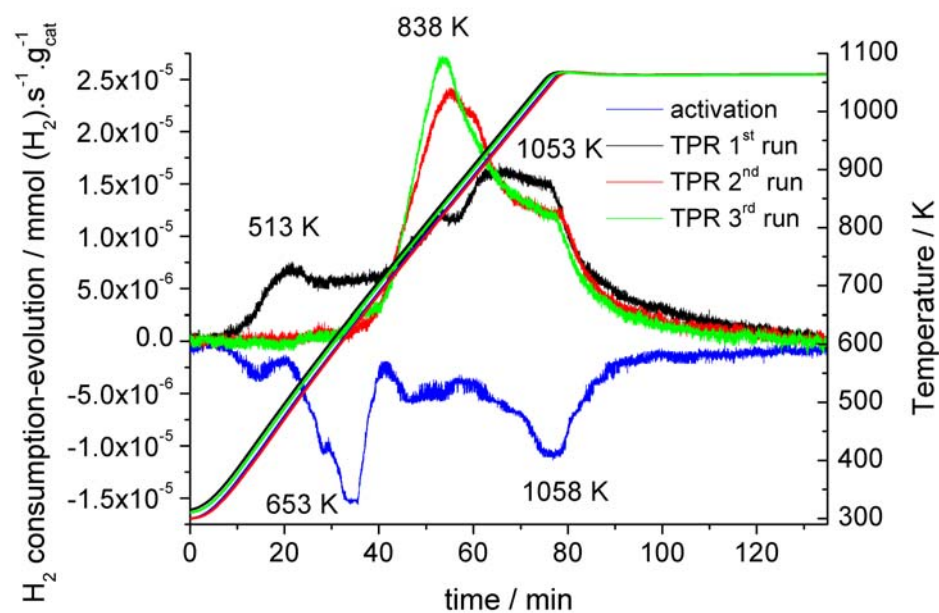
Fig. S3. TPR-O of Fe-MgO. The blue line was measured during pretreatment in 90 mL·min^{-1} Ar applying a heating rate of 10 K·min^{-1}.
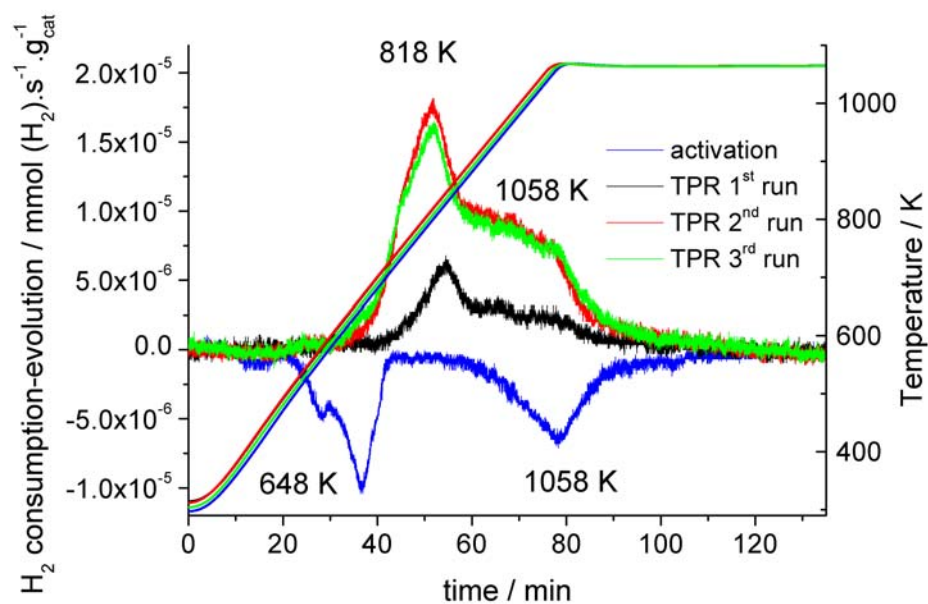
Fig. S4. TPR-O of Au-Fe-MgO. The blue line was measured during pretreatment in 90 mL·min^{-1} Ar applying a heating rate of 10 K·min^{-1}.
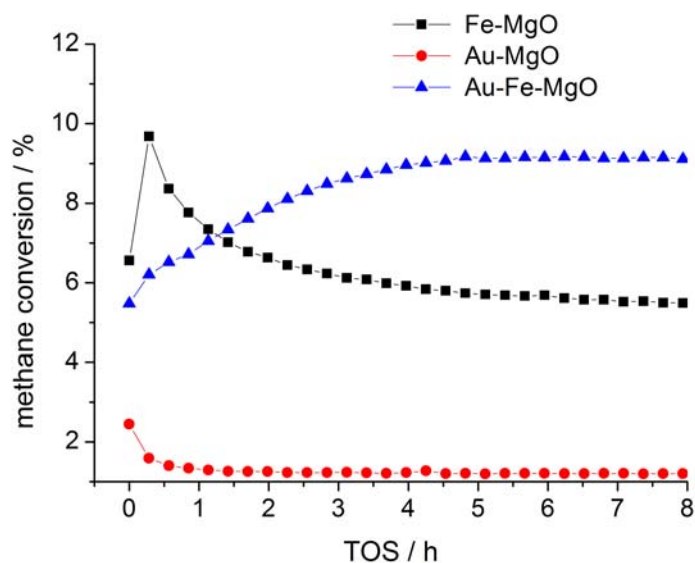
5. Oxidative coupling of methane

Fig. S5 Methane conversion in the oxidative coupling of methane as a function of time on stream (TOS) at T=1023 K; W/F= 0.0167 g·s·ml^{-1}; CH_4/O_2 /N_2=3/1/1.
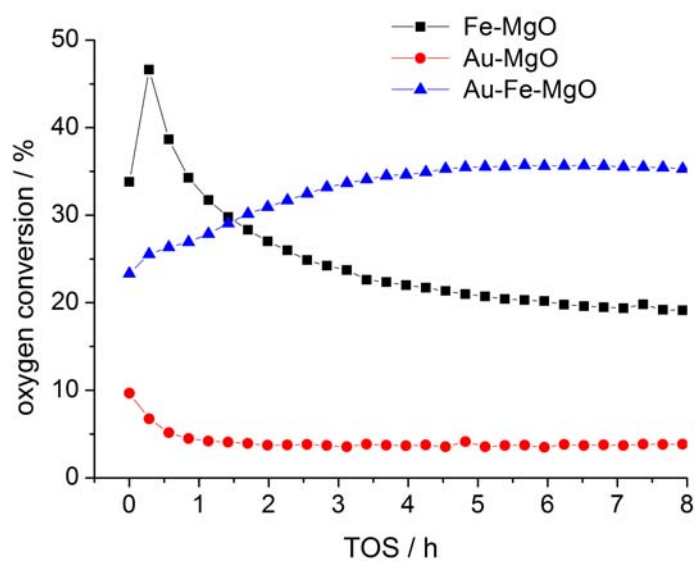

Fig. S6 Oxygen conversion in the oxidative coupling of methane as a function of time on stream (TOS) at T=1023 K; W/F= 0.0167 g·s·ml^{-1}; CH_4/O_2 /N_2=3/1/1.
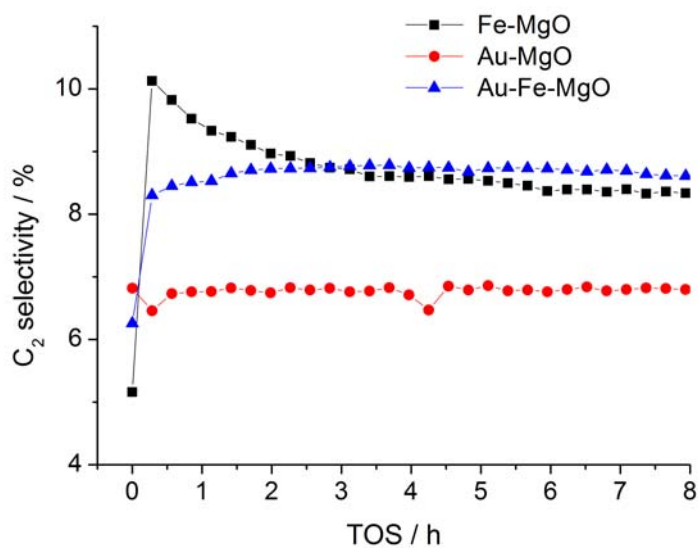
Fig. S7 Selectivity of the sum of ethane and ethene (C_2) in the oxidative coupling of methane as a function of time on stream (TOS) at T=1023 K; W/F= 0.0167 g·s·ml^{-1}; $CH_4/O_2 /N_2$=3/1/1.
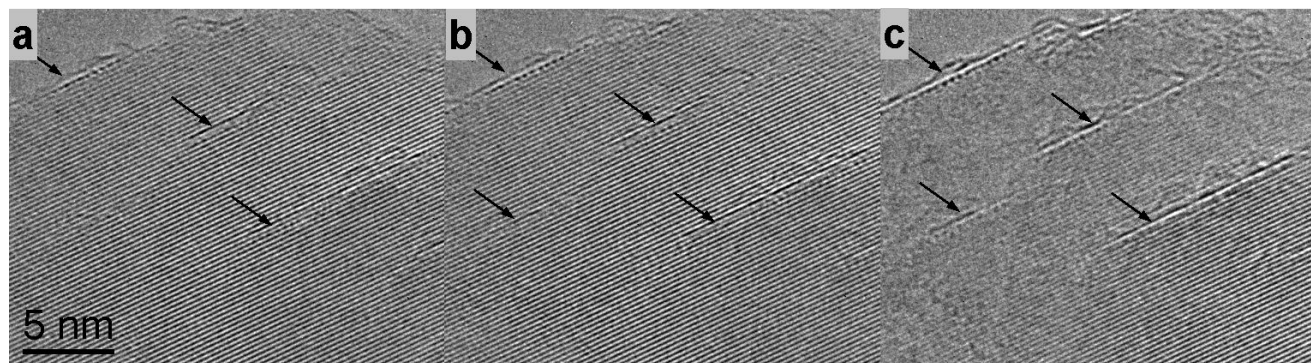
6. Electron microscopy

Fig. S8. Series of HRTEM images recorded at different defocus reveal the presence of strongly scattering atoms located at the steps in the Au-Fe-MgO catalyst after catalysis.